Contents lists available at ScienceDirect

Chemical Engineering Research and Design

journal homepage: www.elsevier.com/locate/cherd

An equation-oriented novel approach for modeling the falling film absorber using rigorous thermodynamic and transport description

Licianne P.S. Rosa[a,b], *Karen V. Pontes*[a,*], *Glória M.N. Costa*[a], *Alberto T. Penteado*[b], *Erik Esche*[b], *Jens-Uwe Repke*[b]

[a] *Industrial Engineering Graduate Program/Federal University of Bahia. Programa de Pós-Graduação em Engenharia Industrial, EscolaPolitécnica, Universidade Federal da Bahia, Rua Aristides Novis, n° 02, Federação, Salvador 40.210-630 BA, Brazil*

[b] *Process Dynamics and Operations Group, Technische Universität Berlin, Sekretariat KWT 9, Straße des 17. Juni 135, 10623 Berlin, Germany*

ARTICLE INFO

Article history:
Received 17 December 2019
Received in revised form 20 March 2020
Accepted 2 April 2020
Available online 20 April 2020

Keywords:
Differential algebraic model
Falling film absorber
Ammonia and water

ABSTRACT

Falling liquid films are largely employed in heat and mass transfer processes in a variety of industrial systems, including absorption processes using NH_3 and H_2O as working fluid. This study develops a new approach based on differential algebraic model for the absorption of NH_3 from a gaseous stream by a solution of NH_3 and H_2O in a falling film absorber at steady-state. Unlike the usual approach in literature, wherein sequential algorithms are specifically tailored to solve the model, the full set of differential algebraic equations (DAE) has been formulated and solved in an equation-oriented fashion. A rigorous modeling of the vapor–liquid equilibrium at the interface is proposed and compared with the usually employed empirical correlations. Thermal and transport properties (TTP) are computed by CAPE-OPEN interfaces, providing robustness and flexibility to the model. The TTP and the falling film model are validated with experimental data from literature. The results indicate that the liquid falling film imposes the dominant mass transfer resistance compared to the gas phase, whereas the coolant-side imposes the dominant heat transfer resistance. The simultaneous solution of the DAE system is very efficient, robust and flexible, as it can be applied for absorbers with different geometries and working fluids.

1. Introduction

There is a significant requirement for refrigeration at deep-freezing temperatures in a variety of industrial segments such as chemical, pharmaceutical, and food processing. In order to achieve low temperatures in industrial systems, one of the most commonly used refrigeration cycle is the absorption refrigeration system (Flori and Vîlceanu, 2012). The absorber is the most critical unit operation for the overall performance (Lázaro-Colán, 2012; Mittermaier and Ziegler, 2015). In the absorber, the refrigerant at the vapor phase is absorbed by an absorbent solution and desorbed in an upstream equipment in a highly endothermic process, producing the refrigerant at deep-freezing temperatures. A lot of research has gone into the development of the working fluid since its properties largely influence the performance and efficiency of the absorption refrigeration system. A wide variety of refrigerant-absorbent combinations, both organic and inorganic, have been suggested for vapor absorption cooling systems. The two most common working fluids in absorption refrigeration

* *Corresponding author.*
E-mail address: karenpontes@ufba.br (K.V. Pontes).
https://doi.org/10.1016/j.cherd.2020.04.006

Nomenclature

A	area (m^2)
z	length (m)
δ	thickness of the film (m)
m	mass flowrates ($kg\,s^{-1}$)
$\dot{n}$	mass flux $kg.m^{-2}\,s^{-1}$
U	overall heat transfer coefficient though the wall ($W\,m^{-2}\,K^{-1}$)
q	sensible heat flux ($W\,m^{-2}$)
H	enthalpy ($J\,kg^{-1}$)
$\tilde{h}$	partial mass enthalpy ($J\,kg^{-1}$)
Q	heat flux ($W\,m^{-2}$)
L	length of the heat and mass exchange area
P	pressure (bar)
R	ideal gas constant ($cm^3\,atm^{-1}\,mol^{-1}$)
T	temperature (K)
d	diameter (m)
x	molar/mass fraction at the liquid phase
y	molar/mass fraction at the vapor phase
α	heat transfer coefficient ($W\,m^{-2}\,K^{-1}$)
F	mass transfer coefficient ($kg\,m^{-2}\,s^{-1}$)
Z	mass fraction of ammonia in the absorbed/desorbed flux
ψ	correction factor
C_P	specific heat ($J\,kg^{-1}\,K^{-1}$)
M	molecular weight ($g\,mol^{-1}$)
Sc	Schmidt number
Pr	Prandtl number
D	diffusivity ($m\,s^{-2}$)
μ	viscosity ($Pa\,s^{-1}$)
λ	thermal conductive ($W\,m^{-1}\,K^{-1}$)
ρ	density ($kg\,m^{-3}$)
Re	Reynolds number
H'	Henry's constant (bar)
v	partial molar volume
f	fugacity (bar)
γ	activity coefficient
a_{22}	parameter of the equation of state
b	parameter of the equation of state
φ	fugacity coefficient
ap	correlation composition parameter
mp	correlation composition parameter
np	correlation composition parameter
nd	number of discretization points
k	numbers of parameters at the empirical correlation for bubble point
j	numbers of parameters at the empirical correlation for dew point

Superscripts

*	asymmetric convention
S	saturation state
P_0	reference pressure
∞	infinite dilution

Subscripts

hv	hydraulic diameter of the vapor in the control volume
0	reference state
L	liquid phase
V	vapor phase
c	coolant
i	component index
int	interface
W	absorber length (m)
w	wall

cycles are $LiBr/H_2O$ and NH_3/H_2O due to their excellent thermal properties that make them capable to be used in cooling systems at commercial scale (Ariyadi and Coronas, 2016). The design of the absorber also plays an important role on the performance and efficiency of the system. The most common are falling liquid films and packed columns. Among them, falling film absorbers have received much attention by researchers due to their applications in many modern devices.

Many numerical and analytic studies have been performed about falling film absorbers with ammonia and water as working fluids. Killion and Garimella (2001) presented a review of the mathematical models that couple heat and mass transfer phenomena in falling film absorption. The authors show a detailed review of the governing equations, solution methods, boundary conditions, simulations and validation as well. Kang et al. (2000) model a plate-type vertical absorber falling film, wherein the aqueous ammonia solution flows counter-currently to the vapor (ammonia) and the coolant (ethylene glycol), validating the results against experimental data. Goel and Goswami (2005b) investigated the combined heat and mass transfer process in a horizontal tube-type falling film absorber. Bohra (2007) conducted a detailed investigation of ammonia-water absorption heat and mass transfer in a horizontal-tube falling-film absorber, reporting experiments and modeling results. Triché et al. (2016) modeled an ammonia-water falling film absorber, which is a corrugated plate heat exchanger, considering coupled heat and mass transfer. The model predictions are validated with experimental data. Aminyavari et al. (2017) presented a model for a concurrent in-tube vertical falling film absorption system to predict the simultaneous heat and mass transfer phenomena in the absorber. The authors validate their model against experimental data obtained from an AHT (Absorption Heat Transformers) absorber.

The usual numerical approach in literature to model the falling film process is to consider finite control volume for the balances, yielding a set of algebraic equations, which are solved sequentially and iteratively by tailored sequential algorithms (Goel and Goswami, 2005a,b; Sieres and Fernandez-Seara, 2007; Triché et al., 2016, 2017; Aminyavari et al., 2017). There is no attempt to obtain a differential model which has to be discretized by, e.g., finite differences, as the current equation-oriented approach. Many authors who have modeled a NH_3/H_2O falling film absorber have used similar sequential approaches (Goel and Goswami, 2005a,b; Sieres and Fernandez-Seara, 2007; Triché et al., 2016, 2017; Aminyavari et al., 2017). Goel and Goswami (2005a), for example, proposed an algorithm, which for a given initial guess of the coolant temperature, computes the equations describing the liquid and vapor differential segments sequentially from the top to the bottom. This procedure is repeated for different guesses of the coolant temperature, given by the average of the inlet and outlet coolant temperatures, until all unknown variables converge to a given tolerance. According to Sieres and Fernandez-Seara (2007), this numerical approach may fail to converge due to the asymptotic discontinuity of the molar

fluxes at the interface. Therefore, the corresponding concentration profiles during the heat and mass transfer processes have to be properly predefined. To skip the asymptotic discontinuity of the molar fluxes, Aminyavari et al. (2017) suggest to compute the molar fluxes by the basic equations presented by Bird et al. (2006) and Treybal (1980) and used e.g. by Kim et al. (2003). Despite of that, these authors still employed the sequential approach proposed by Goel and Goswami (2005a).

This paper aims to develop a model described by differential mass and energy balances coupled with algebraic equations representing the mass and energy transfer as well as the phase-equilibrium at the interface. The resulting set of equations consists of complex and high non-linear differential algebraic equations (DAE). For the first time, an equation-oriented approach is proposed to solve the falling-film absorber simultaneously. One contribution of this paper, therefore, is to formulate a unique set of DAE, which is discretized by the finite differences, and solved simultaneously by standard residual minimization algorithms without the need to program specific procedures such as tearing-sequences. This approach is more systematic and requires a good initialization of the equation system's iteration variables along the absorber height but allows for a more efficient solution because it overcomes state-of-the-art numerical problems. The equation oriented-approach further provides flexibility to the model as it can be easily integrated into flowsheet simulations and large-scale simultaneous optimization problems. The proposed model is validated with experimental data from Triché et al. (2016) for a vertical falling film with corrugated plates, wherein the vapor and the refrigerant flow co-currently (from the top to the bottom), whereas the coolant fluid flows counter-currently (from the bottom to the top).

The phase equilibrium is usually described by simplified empirical correlations proposed by Pretek and Klomfar (1995) for the ammonia-water system to predict the compositions at the interface at a given temperature and pressure for a narrow composition range (Conde, 2006; Triché et al., 2016, 2017). However, a more general representation, which can be extended to other working fluids, might be obtained if a rigorous thermodynamic model is employed. For the ammonia-water system, for example, the equilibrium model proposed by Prausnltz et al. (1978) accurately describes the vapor–liquid equilibrium over the entire composition range. The flexible model formulation proposed herein allows for the inclusion of either the empirical correlations or the rigorous equilibrium model at the interface. The underlying thermodynamic model might be changed accordingly to describe different components and the non-idealities of the vapor and liquid phases. This gives flexibility to the numerical approach and therefore is another contribution to the usual approach found in literature.

When modeling falling films absorbers, the prediction of Thermodynamic and Transport Phenomena Properties (TTP), such as specific heat, specific enthalpy, partial mass enthalpy, binary diffusivity, viscosity, thermal conductivity, and density, also plays a key role in the accuracy of the model. Despite that, the authors do not clearly state which TTP are used in the falling film model (Goel and Goswami, 2005a,b; Sieres and Fernandez-Seara, 2007; Triché et al., 2016, 2017; Aminyavari et al., 2017) and do not attempt to previously validate the TTP against experimental data. Although the system NH_3/H_2O is well known in literature, the calculation of its TTP is still rather scattered. The current model accesses libraries in TEA (Thermodynamics for Engineering Applications) via CAPE-OPEN Interface Standard (CoLan, 2011) to compute the TTP, which are validated against experimental data from literature to ensure precision of the falling film model. Therefore, another contribution of this paper is to discuss and validate the TTP.

The paper is organized as follows. First, in Section 2 the model of the falling film absorber is presented based on the main assumptions, material and energy balances and the equilibrium at the interface. Section 3 illustrates the validation of the model against experimental data from literature and also shows the simulation of temperature and concentrations profiles along the length of the absorber, allowing to analyze how the inlet conditions influence the absorption performance. The results section further discusses the dominant resistances to mass and energy transfer. The paper ends with the conclusion.

2. Mathematical modeling

The NH_3/H_2O falling film absorber might be designed with vertical pipes, vertical plates (Fig. 1a), horizontal pipes, etc. Regardless of the geometry, the absorption principle is the same: vapor of ammonia (refrigerant) is absorbed by the NH_3/H_2O solution (absorbent). Since the absorption is an exothermic process, water or another refrigerant is used as coolant to avoid an undesired temperature increase in the liquid phase in order to keep the liquid solution far from the boiling point and to sustain the absorption process as well.

Some assumptions may be considered when modeling falling film absorbers, as also suggested by Aminyavari et al. (2017) and Triché et al. (2016, 2017):

- The flows of heat, liquid and gas are assumed to be equally distributed through the plates of the falling film absorber;
- The flow is one-dimensional and in steady-state;
- The flow is well-established at the inlet;
- The heat losses to the environment are neglected (insulated or adiabatic equipment);
- No chemical reaction is taking place;
- Gas/vapor and liquid are in equilibrium at the interface;
- The heat and mass transfer surfaces are equal and the heat and mass transfer resistances are confined to a thin region close to the interface;
- The only driving force for the mass transfer is the concentration difference between the liquid solution and the gas/vapor, i.e., mass transfer due to pressure and temperature difference is neglected;
- The pressure drop is neglected.

A differential control volume (CV) is illustrated in Fig. 1b. The positive sign convention for heat and mass fluxes is adopted, meaning that the heat and mass fluxes flow from the vapour phase to the liquid phase and heat, from the liquid phase to the coolant. The vapour and liquid streams are fed at the top, whereas the coolant flows counter-currently. When the liquid and vapour phases come into contact, the absorption/desorption occurs.

The mass and energy balances are written for an infinitesimal volume with length dz. The infinitesimal area of the interface where mass and heat transfer between liquid and vapor occurs is given by:

$$dA_i = L \cdot dz \tag{1}$$

where L is the length of the heat and mass exchange area and dz is the height of the infinitesimal element. If the falling-film

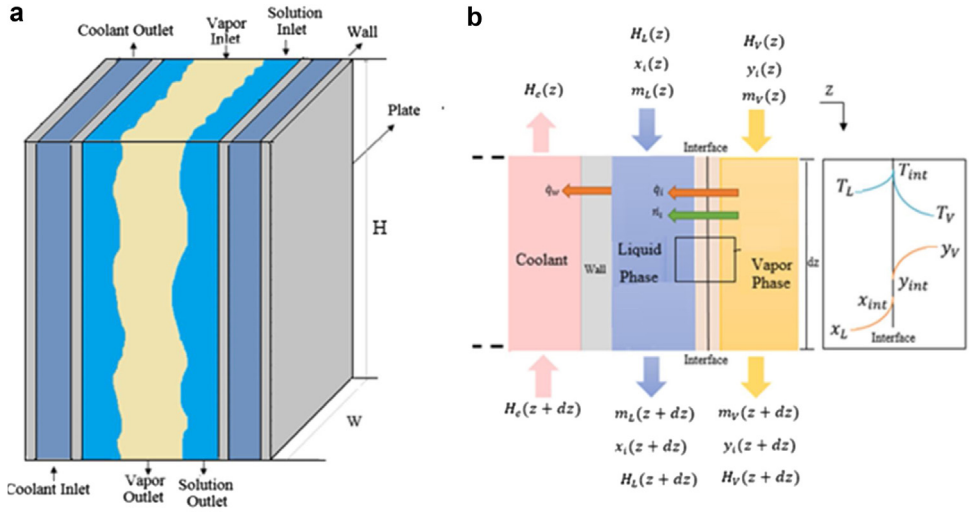

Fig. 1 – (a) Plates falling film absorber and (b) differential control volume (CV) (adapted from Triché et al., 2016).

Table 1 – Mass, component and energy balances at the CV.

Vapor phase	
Mass balance	$\frac{dm_V}{dz} = -L\sum_{i-1}^{NC}\dot{n}_{i,int}$
Component mass balance	$\frac{d(m_V y_i)}{dz} = \frac{d(m_{V,i})}{dz} = -\dot{n}_{i,int}L \quad i = 1,\ldots,NC$
Energy balance	$\frac{dH_V}{dz} = \frac{(-\dot{q}_V + H_V\sum_{i=1}^{NC}\dot{n}_{i,int})L}{m_V}$
Liquid phase	
Mass balance	$\frac{dm_L}{dz} = L\sum_{i-1}^{NC}\dot{n}_{i,int}$
Component mass balance	$\frac{d(m_L y_i)}{dz} = \frac{d(m_{L,i})}{dz} = -\dot{n}_{i,int}L \quad i = 1,\ldots,NC$
Energy balance	$\frac{dH_L}{dz} = \frac{(\dot{q}_L + H_L\sum_{i=1}^{NC}\dot{n}_{i,int})L - L_c U(T_L - T_c)}{m_L}$
Coolant	
Energy balance	$\frac{dH_c}{dz} = -\frac{L_c Q_c}{m_c} = -\frac{L_c U(T_L - T_c)}{m_c}$
Boundary conditions	
$m_L(z=0) = m_{L0}$	$m_V(z=0) = m_{V0}$
$m_L(z=0) = m_{L0}$	$y_i(z=0) = y_{i0}$
$x_i(z=0) = x_{i0}$	$x_i(z=0) = x_{i0}$
$H_L(z=0) = H_{L0}$	$H_V(z=0) = H_{V0}$
	$H_c(z=L) = H_{cL}$

is constituted of pipes, for example, $L = \pi(d - 2\delta)$ where d is the inner diameter of the pipe, δ (m) is the thickness of the film. If the falling-film is constituted of plates, $L = W$, where W is width of the plates. The falling film absorber modeled here is a corrugated plate heat exchanger presented by Triché et al. (2016). It can be represented by Fig. 1b, where gas and liquid flow between every two plates. More details about the geometry and measurement devices can be found in Triché et al. (2016). The falling film absorber is modeled by mass, component, and energy balances of the liquid, vapor and coolant phases, as well as heat and mass transfer equations at the interface and thermodynamic equilibrium at the interface. The next sections describe each part of the model proposed here.

2.1. *Material and energy balances at the bulk phases and at the coolant*

The mass, component, and energy balances for each phase, vapor, liquid, as well as the coolant in the CV (Fig. 1b) are summarized in Table 1. In Table 1, L is the total length of the heat and mass exchange area, NC is the number of components, z is the length (m), m_L and m_V are the liquid and vapor mass flowrates (kg s^{-1}), $\dot{n}_{i,int}$ is the mass flux of component i (kg m^{-2} s^{-1}), which is calculated by the mass transfer equations at the interface, y_i and x_i are mass fractions of component i at the gas and liquid phases, respectively; T_L is the bulk liquid temperature (K); T_c is the coolant temperature (K); L_c is the length of the heat exchange area for the coolant; m_c is coolant mass flowrate (kg s^{-1}); H_c (J kg^{-1}) is coolant enthalpy; Q_c (W m^{-2}) is coolant heat flux; U is the overall heat transfer coefficient for the wall (W m^{-2} K^{-1}); $\dot{q}_V$ and $\dot{q}_L$ are the sensible heat fluxes (W m^{-2}) for the vapor and liquid phases calculated at the interface. The enthalpy of liquid mixture, H_L (J kg^{-1}), is computed by the correlation proposed by Pretek and Klomfar (1995), as already applied by others (Conde, 2006; Triché et al., 2016, 2017), according to:

$$H_L = h_0\sum_i a_i\left(\frac{T}{T_0} - 1\right)^{m_i} x_{NH_3}^{n_i} \quad (2)$$

Table 2 – Heat and mass transfer equations at the interface.

Mass flux at the vapor interface	$\sum_{i-1}^{NC} \dot{n}_{i,int} = K_V \rho_V \ln \frac{(Z - y_{NH_3,int})}{(Z - y_{NH_3})}$
Mass flux at the liquid interface	$\sum_{i-1}^{NC} \dot{n}_{i,int} = K_L \rho_L \ln \frac{(Z - x_{NH_3})}{(Z - x_{NH_3,int})}$
Heat transfer equation at the interface	$\dot{\alpha}_V (T_V - T_{int}) + \sum_{i-1}^{NC} \dot{n}_{i,int} \tilde{h}_{V,i} = \dot{\alpha}_L (T_{int} - T_L) + \sum_{i-1}^{NC} \dot{n}_{i,int} \tilde{h}_{L,i}$

where T is the temperature, x_{NH_3} is the ammonia mass fraction in liquid phase, $h_0 = 100$ (kJ kg^{-1}) is the reference enthalpy, $T_0 = 273.16$ (K) is the reference temperature and the parameters a_i, m_i and n_i are given in Pretek and Klomfar (1995). The gas phase is assumed to behave as an ideal mixture, so that the enthalpy (H_V, J kg^{-1}) might be computed as:

$$H_V = \sum_i x_i h_{V,i} \tag{3}$$

where x_i is composition of component $i \in \{NH_3, H_2O\}$ in liquid phase and $h_{V,i}$ is the specific enthalpy of the pure components $i \in \{NH_3, H_2O\}$, given by:

$$h_{V,i} = \int_{T_0}^{T} C_{PV,i} dT \tag{4}$$

where T (K) is temperature, T_0 is reference temperature and $C_{PV,i}$ is the specific heat capacity of component i computed using correlations from literature, which are summarized in Appendix A.

2.2. *Mass and heat transfer equations at the interface*

The simultaneous heat and mass transfers and the dominant transfer resistance, i.e., which phase offers the highest resistance to mass and energy transfers, are key aspects in the mathematical modeling of falling film absorbers. The knowledge of the dominant transfer resistance allows ascertaining the limiting steps to the absorption process. Many studies on absorption modeling consider heat and mass transfers separately, reasoning that there is negligible heat interaction so that the process might be considered isothermal (Vyazovov, 1940; Cosenza and Vliet, 1990; Deng and Ma, 1999; Miller and Keyhani, 2001). Chen et al. (2010), on the other hand, state that the mass exchange increases/decreases the liquid temperature at the interface accordingly, consequently influencing the equilibrium states and the mass transfer. The heat and mass transfer, therefore, should be considered simultaneous (Grossman, 1983; Kim, 1998; Habib and Wood, 2001; Ho et al., 2004; Goel and Goswami, 2005a,b; Sieres et al., 2007; Triché et al., 2016, 2017; Aminyavari et al., 2017). There is disagreement in literature regarding the dominant mass transfer resistance. Potnis et al. (1997), Gommed et al. (2001) and Aminyavari et al. (2017) conclude that the vapor phase offers the dominant transfer resistance. On the other hand, Kang et al. (1998, 2000), Goel and Goswami (2005a,b), Fernandez-seara et al. (2005), Sieres and Fernandez-Seara (2007), Lin and Xia (2011) and Triché et al. (2017) conclude that the liquid phase offers the dominant transfer resistance for the mass transfer. Given the uncertainty of the relative magnitude of the mass resistance in the liquid and gas phases, both contributions (gas and liquid) are considered in this study. This investigation is fundamental to understand which phase (liquid or vapor) controls the mass and heat transfer phenomenon on the absorption process.

Taking into account that there is no mass accumulation and no reaction at the interface, continuity of the total mass and heat flux at the interface might be assumed for any components being transferred, then:

$$\dot{n}_{i,L} = \dot{n}_{i,V} = \dot{n}_{i,int} \quad i =, \ldots, NC \tag{5}$$

$$\dot{q}_L = \dot{q}_V = \dot{q}_{int} \tag{6}$$

where $\dot{n}$ (kg m^{-2} s^{-1}) and $\dot{q}$ (W m^{-2}) are the mass and heat fluxes respectively, i indicates the component, NC is the number of components, the subscripts L and V represent the vapor and liquid phase respectively, and int indicates the interface.

The heat and mass transfer equations at the vapor–liquid interface are then summarized in Table 2, where K_L (m s^{-1}) and K_V (m s^{-1}) are the mass transfer coefficients of the liquid and the vapor phase respectively; ρ_V and ρ_L are the densities of vapor and liquid phases respectively (kg m^{-3}); $\dot{n}_{i,int}$ (kg m^{-2} s^{-1}) is the mass flux of components i; $\dot{\alpha}$ (W m^{-2} K^{-1}) is the heat transfer coefficient; x_i and y_i are the mass fractions of component i at the liquid and vapor bulk respectively and $x_{i,int}$ and $y_{i,int}$ are the liquid and vapor mass fractions of component i at the interface. The partial mass enthalpies for the component i in liquid phase, $\tilde{h}_{L,i}$ (J kg^{-1}), are computed according (Ziegler and Trepp, 1984):

$$\tilde{h}_{L,i} = H_L + x_i \frac{\partial H_L}{\partial x} \tag{7}$$

where x_i is mass fraction of component $i \in \{NH_3, H_2O\}$ in liquid phase and H_L is the mass enthalpy of liquid mixture. The partial mass enthalpies for the component i in vapor phase, $\tilde{h}_{V,i}$, are considered equal to the specific enthalpies of the pure components, $h_{V,i}$, because at low pressures the non-ideal behavior of the vapor phase is negligible. Z is the mass fraction of ammonia in the absorbed/desorbed flux, expressed as (Treybal, 1980):

$$Z = \frac{\dot{n}_{NH_3}}{\sum_I^{NC} \dot{n}_{i,int}} \tag{8}$$

The value of Z indicates the variation of exchanged mass fluxes along the absorber. For an absorption involving NH_3/H_2O mixture in vapor and in liquid phase, for example, if Z is greater than 1, water is desorbed from liquid into vapor ($\dot{n}_{H_2O} < 0$) and, if Z is less than 1, water is absorbed from vapor into liquid ($\dot{n}_{H_2O} > 0$). In summary, positive values of the mass

flux indicates absorption from vapor into liquid and negative values of mass flux indicate desorption from liquid into vapor.

The mass fluxes of ammonia and water, $\dot{n}_{i,int}$ ($kg\,m^{-2}\,s^{-1}$), are calculated according to Treybal (1980), as also carried out by Goel and Goswami (2005a,b), Lin and Xia (2011), Sieres and Fernandez-Seara (2007). The equations are presented in Table 2, given the composition at the interface and at the liquid and vapor bulk concentrations. Regarding the heat fluxes at the interface, they consist of two parts: the convective heat transfers due to the temperature gradient between both phases and the sensible heat transfer due to the mass transfer across the interface (Bird et al., 2006).

The algorithm proposed by Sieres and Fernandez-Seara (2007) uses Z and the compositions at the interface as tear-variables, thus suitable initial guesses are required for these variables. However, the authors point out that their algorithm may fail if the combination of these guess values makes the logarithmic terms not defined. Aminyavari et al. (2017) try to overcome this numerical problem using another correlation to compute the fluxes at the interface, without defining Z. The simultaneous approach proposed herein does not require any equation tearing, as detailed in Section 2.5, then it can efficiently solve the falling film model using the equations in Table 2, although they depend on Z.

2.3. Mass and heat transfer coefficients

The heat transfer coefficient for the liquid phase, $\dot{\alpha}_L$ ($W\,m^{-2}\,K^{-1}$) can be calculated using the Chilton and Colburn (1934) analogy:

$$\dot{\alpha}_L = \psi_{hL}\alpha_L \tag{9}$$

$$\alpha_L = K_L\left(C_{PL}M_L\left[\frac{SC_L}{Pr_L}\right]^{2/3}\right) \tag{10}$$

where M_L ($kg\,mol^{-1}$) is molecular weight, K_L ($m\,s^{-1}$) is the mass transfer coefficient for the liquid phase, C_{PL} ($J\,kg^{-1}\,K^{-1}$) is the specific heat capacity of the liquid mixture and is calculated assuming the ideal mixture law, as recommended by Conde (2006), Prata (2012) and Leite (2015). The specific heat capacity of the pure components $C_{PL,i}$ is computed according to Perry and Green (1999). Pr_L is the Prandtl number $\left(Pr_L = \frac{\mu_L C_{P,L}}{\lambda_L}\right)$ and SC_L is the Schmidt number $\left(SC_L = \frac{\mu_L}{D_L\rho_L}\right)$, where D_L is the binary diffusivity for the liquid phase, computed according to (Wilke and Chang, 1955), μ_L is the viscosity ($Pa\,s^{-1}$), λ_L ($W\,m^{-1}\,K^{-1}$) is the thermal conductivity and ρ_L ($kg\,m^{-3}$) is the density. The correction factor, ψ_{hL}, takes into account the finite mass transfer effect and is calculated according to (Triché et al., 2016):

$$\psi_{hL} = \frac{\left(\sum_{i=1}^{NC}\dot{n}_{i,int}C_{PL,i}/\alpha_L\right)}{1-e^{\left(\sum_{i=1}^{NC}\dot{n}_{i,int}C_{PL,i}/\alpha_L\right)}} \tag{11}$$

The heat transfer coefficient for the vapor phase, $\dot{\alpha}_V$ ($W\,m^{-2}\,K^{-1}$), can be calculated from the correlation given by Kakaç et al. (1987):

$$\dot{\alpha}_V = \psi_{hV}\alpha_V \tag{12}$$

$$\alpha_V = 7.541\left(\frac{\lambda_V}{d_{hv}}\right) \tag{13}$$

where λ_V ($W\,m^{-1}\,K^{-1}$) is the thermal conduction in the vapor phase, d_{hv} (m) is hydraulic diameter of the vapor in the control volume. This correlation is valid if $Re < 2200$ and fully developed conditions. The correction factor (ψ_{hV} is calculated by (Triché et al., 2016):

$$\psi_{hv} = \frac{\left(\sum_{i=1}^{NC}\dot{n}_i C_{PV,i}/\alpha_V\right)}{1-e^{\left(\sum_{i=1}^{NC}\dot{n}_i C_{PV,i}/\alpha_V\right)}} \tag{14}$$

The mass transfer coefficient for the vapor phase K_V ($m\,s^{-1}$) can also be calculated by applying the Chilton and Colburn (1934) analogy:

$$K_V = \frac{\alpha_V}{C_{PV}M_V[SC_V/Pr_V]^{2/3}} \tag{15}$$

where M_V ($kg\,mol^{-1}$) is molecular weight, α_V ($m\,s^{-1}$) is heat transfer coefficient for the vapor phase (Eq. (13)), C_{PV} ($J\,kg^{-1}\,K^{-1}$) is the ideal gas specific heat capacity of the mixture. The specific heat for the pure components $C_{PV,i}$ is taken from Van Ness et al. (2007). Pr_V is the Prandtl number ($Pr_V = (\mu_V C_{PV}/\lambda_V)$), Sc_V is the Schmidt number ($Sc_V = (\mu_V C_V \rho_V)$), where D_V is binary diffusivity for the vapor phase (Wilke and Chang, 1955), μ_V is viscosity ($Pa\,s^{-1}$), λ_V is thermal conductive and ρ_V ($kg\,m^{-3}$) is density.

The mass transfer coefficient, K_L ($m\,s^{-1}$) between the liquid phase and the interface is obtained from the correlation developed by Yih (1986). This equation is only valid in a falling film with a Reynolds number between 49 and 300 and in fully developed conditions (Triché, 2016). It may be calculated by:

$$K_L = 0.01099Re_{film}^{0.3955}Sc_L^{0.5}\left(\frac{D_L\rho_L}{M_L}\right)\left[\frac{g\rho_L^2}{\mu_L^2}\right]^{1/3} \tag{16}$$

where Re_{film} is the Reynolds number for the liquid film, Sc_L Schmidt number for the liquid phase, M_L is the molecular weight ($kg\,mol^{-1}$), D_L is binary diffusivity, μ_L is viscosity ($Pa\,s^{-1}$), ρ_L is density ($kg\,m^{-3}$).

The Thermodynamics and Transport Phenomena Properties (TTP), namely viscosity ($Pa\,s^{-1}$), thermal conductivity ($W\,m^{-1}\,K^{-1}$), and density ($kg\,m^{-3}$) for the pure components in liquid and vapor phases as well as for the liquid mixture, are calculated by the software TEA (Thermodynamics for Engineering Applications, Van Baten, 2016) via CAPE-OPEN interfaces. CAPE-OPEN is a set of software interfaces standardized for plug and play inter-operability between a given process modeling environment and a third-party process modeling component (CoLan, 2011). The property packages TEA offers a number of different methods to compute the TTP. The embedded methods listed in Table 3 are choose due to their suitability to the system and to the operating conditions studied. This choice might be easily changed according to the system and its operating conditions. The use of CAPE-OPEN interfaces might be used in any process model so that the user can, on the one hand, concentrate on the development of the model itself and, on the other hand, have access to a variety of methods to compute the TTP for different components and operating conditions. This approach, then, provides great flexibility to the model.

The specific heats of pure components and mixture as well as the binary diffusivity coefficients for liquid and vapor phases are computed using correlations from literature, which are summarized in Appendix A.

Table 3 – Correlations for TTP prediction in TEA.

Property	Pure components		Mixture	
	Liquid	Vapor	Liquid	Vapor
Density	COSTALD/ Hankinson and Thompson	EOS-Soave Redlich Kwong	COSTALD/ Hankinson and Thompson	EOS-Soave Redlich Kwong
Viscosity	Letsou- Stiel Method: Temperature Correlation	Yoon and Thodos method	Logarithmic mixing (mass based)	Brokaw
Thermal conductivity	Pachaiyappan Method	DIPPR procedure 9B-1	Ideal	Ideal

The overall heat transfer coefficient for the wall is given by:

$$U = \frac{1}{(1/\alpha_{L,w}) + R_w + (1/\alpha_c)} \tag{17}$$

where R_w ($W\,m^{-2}\,K^{-1}$) is the conductive resistance of the plate made of inox, $\alpha_{L,w}$ ($W\,m^{-2}\,K^{-1}$) is the heat transfer coefficient between the liquid film and the plate given by $\alpha_{L,w} = 1.88\frac{\lambda_L}{\delta_{film}}$ (Wilke, 1962), for $Re < 2469\ Pr^{-0.646}$ and fully developed conditions, where λ_L ($W\,m^{-1}\,K^{-1}$) is the thermal conductivity, δ_{film} (m) is the falling film thickness. α_c ($W\,m^{-2}\,K^{-1}$) is the heat transfer coefficient between the coolant and the plate, calculated by $\alpha_c = 4.363\frac{\lambda_c}{D_h}$ (Goel and Goswami, 2005a), for fully developed laminar flow conditions, where λ_c ($W\,m^{-1}\,K^{-1}$) is thermal conductive and D_h is hydraulic diameter.

2.4. *Equilibrium at the interface*

Liquid and vapor compositions at the interface, $x_{i,int}$ and $y_{i,int}$, are calculated from phase equilibrium at the interface. According to Seader and Henley (1998), it is necessary to know whether the components dissociate during the absorption process. Since ammonia is a weak electrolyte, it ionizes appreciably in a large excess of water, according to:

$$NH_3 + H_2O \leftrightarrow NH_4^+ + OH^- \tag{18}$$

If the liquid phase is a diluted solution, the phase equilibrium for weak electrolytes might be modeled as Edwards et al. (1975, 1978). When the ammonia molar fraction in the liquid phase is above 10^{-3}, though, the ionization is negligible (Prausnltz et al., 1978). Since the ammonia molar fraction in the studied falling film greatly exceeds 10^{-3} at all points, it is reasonable to assume that there is no dissociation in the liquid phase. There are two approaches to calculate the compositions at the interface for ammonia and water mixture that have been previously proposed in literature: a rigorous thermodynamic model by Prausnltz et al. (1978), which accurately describes the ammonia-water system over the entire composition range; or a simplified empirical correlation for pressures below 20 bar, according to Pretek and Klomfar (1995). A brief comparison is presented in the following.

2.4.1. *Rigorous thermodynamic model*

Some assumptions might be made for the vapor–liquid equilibrium (VLE) of ammonia and water: vapor phase is an ideal gas at the operating temperature and pressure conditions of the studied falling film ($P = 6$ bar and $290 \leq T \leq 365$ K), as also assumed by other authors (Triché et al., 2016); there is no dissociation, so ammonia is not an electrolyte. The vapor–liquid equilibrium for the system ammonia and water are then written as:

$$y'_{NH_3} P = x'_{NH_3} \gamma^*_{NH_3} H' \exp\left(\frac{\bar{v}^{\infty}_{NH_3} P}{RT}\right) \tag{19}$$

$$y'_{H_2O} P = x'_{H_2O} \gamma_{H_2O} f^{P0}_{H_2O,L} \exp\left(\frac{\bar{v}_{H_2O} P}{RT}\right) \tag{20}$$

where y' and x' are molar fraction in vapor and liquid phase, respectively, $\bar{v}_i^{\infty}$ is the partial molar volume at the infinite dilution of component i in the solvent (water), available at Krichevsky and Kasarnovsky (1935), R is the universal gas constant, T is temperature, P is pressure, H' is Henry's constant for molecular ammonia in water, whose values are determined from experimental data in the dilute region (Edwards et al., 1975, 1978), γ_{H_2O} is the activity coefficient of water which is calculated by Prausnltz et al. (1978), $\gamma^*_{NH_3}$ is the activity coefficient of ammonia in a symmetric convection, which is calculated by a hyperbolic tangent function (Prausnltz et al., 1978):

$$\ln(\gamma^*_{NH_3}) = b \cdot \tanh\left(\frac{a_{22} x'_{NH_3}}{b\,(1 - x'_{NH_3})}\right) \tag{21}$$

where x'_{NH_3} is the ammonia molar fraction in liquid phase, the parameter a_{22} is obtained from Prausnltz et al. (1978) and the parameter b is determined by:

$$b = \ln\left(\frac{f^{P0}_{NH_3,L}}{H'}\right) \tag{22}$$

where $f^{P0}_{NH_3,L}$ is the fugacity of pure liquid ammonia at the system temperature, corrected to zero pressure:

$$f^{P0}_{NH_3,L} = \varphi^S_{NH_3} P^S_{NH_3} \exp\left(-\frac{v_{NH_3} P^S_{NH_3}}{RT}\right) \tag{23}$$

where $P^S_{NH_3}$ is the vapor pressure of pure ammonia (Macriss et al., 1964), v_{NH_3} is the molar volume of pure liquid ammonia (Din, 1956) and $\varphi^S_{NH_3}$ is the fugacity coefficient at saturation, determined by the Soave–Redlich–Kwong equation of state. This approach uses rigorous thermodynamic models to describe the VLE, which might be changed accordingly to describe different components and the non-idealities of the vapor and liquid phases.

2.4.2. *Empirical correlations*

Alternatively, it can be assumed that the temperature at the interface is the saturation temperature, so that empirical correlations for bubble and dew point temperatures can be used to compute the compositions at the interface, as carried out

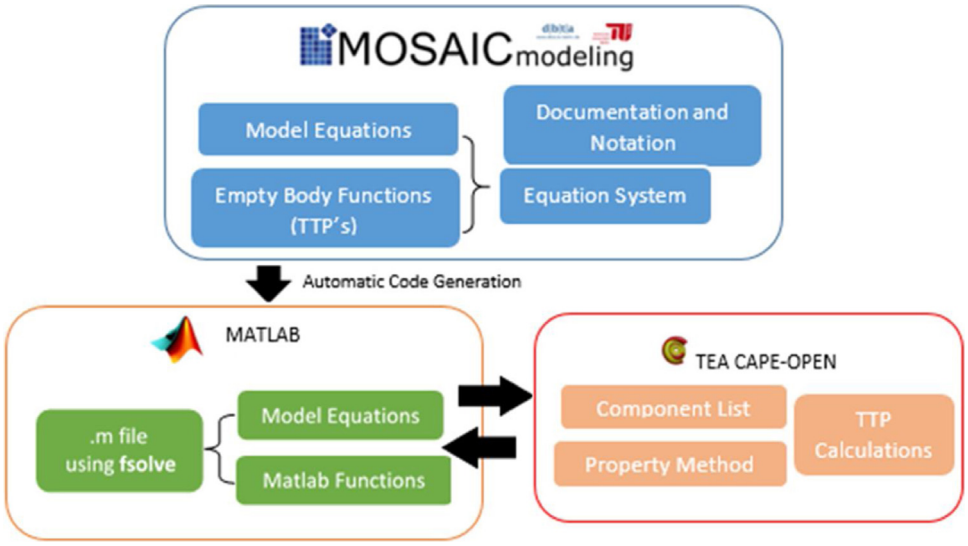

Fig. 2 – Overview of the modeling and simulation framework.

by Conde (2006) and Triché et al. (2016, 2017). The empirical correlations developed by Pretek and Klomfar (1995) for the bubble and dew point temperatures are respectively given by:

$$T(P, x_{NH_3}) = T_0 \sum_{k=1}^{14} ap_k (1 - x_{NH_3})^{mp_k} \left[\ln \frac{P_0}{P}\right]^{np_k} \quad (24)$$

$$T(P, y_{NH_3}) = T_0 \sum_{j=1}^{17} ap_j (1 - y_{NH_3})^{\frac{mp_j}{4}} \left[\ln \frac{P_0}{P}\right]^{np_j} \quad (25)$$

where T is temperature, P is pressure, the subscript 0 indicates the reference state, $T_0 = 100\,K$ and $P_0 = 2\,MPa$, x and y are the mass fraction in liquid and vapor phase, respectively, the parameters ap, mp and np are given by Pretek and Klomfar (1995) for k and j parameters. These correlations are the resulting functions, which best reproduce the selected experimental data ($193.15\,K \leq T \leq 453.15\,K$ and $0.02\,bar \leq P \leq 20\,bar$) used by the authors (Pretek and Klomfar, 1995). Therefore, for a given pressure and temperature at the interface, it is possible to solve the system of algebraic equations (24 and 25) to calculated the interface compositions, x and y.

2.5. *Solution procedure*

The falling film absorber model is represented by a system of differential algebraic equations (DAE), composed by $5 + 2 \cdot NC$ differential equations (Table 1), 3 algebraic equations, which describe the mass fluxes and the temperature at the interface (Table 2) and $NC + 2$ equations to compute the compositions at the interface (Eqs. (19) and (20) or (24) and (25) plus the summation of the mass fractions at each phase). The vector $\mathbf{X}$ represents the algebraic and state variables of the DAE system:

$$\mathbf{X} = [m_L, m_V, \mathbf{x}, \mathbf{y}, H_L, H_v, H_c, \mathbf{n}, T_{int}, \mathbf{x_{int}}, \mathbf{y_{int}}] \quad (26)$$

Since the coolant flows counter-currently to the gas and liquid process streams, boundary conditions are specified for both $z = 0$ and $z = L$ and the system cannot be solved as an initial value problem. The DAE system is, therefore, discretized by the finite differences method (forward for the liquid and vapor side and backward for the coolant side), resulting in a set of $(10 + 3 \cdot NC) \cdot nd$ algebraic non-linear equations, where nd is the number of discretization points considering a uniform grid. One of the challenges of the equation-oriented approach used herein is that the values of all state variables along the absorber length must be properly initialized. This has been done by specification of variables along the absorber, such as enthalpies, mass flow rate etc. The initial guess for the iteration variables was given by simulated data from literature.

The discretized DAE system, i.e. algebraic non-linear system, is implemented in MOSAICmodeling (http://mosaic-modeling.de/), which is a free, web-based modeling environment capable of automatically generating code for process simulation and optimization in different programming languages (Merchan et al., 2015; Tolksdorf et al., 2019). The model is then solved in Matlab using the native function *fsolve*, which is based on the residual minimization method. The TTP are computed via CAPE-OPEN interfaces using the libraries in TEA. The functions, which calculate heat and mass transfer coefficients, are defined as "Empty Body Functions" in MOSAICmodeling. These act as place-holder function calls and definitions in the system of equations. Once MOSAICmodeling generates the code for the solution in Matlab, interfaces with a CAPE-OPEN-compliant property package such as TEA are manually programmed, allowing for the external calculation of TTP, as shown in Rosa et al. (2018). To enable the CAPE-OPEN function calls in Matlab, the plug-in Matlab Thermo Import from AmsterCHEM is used (Van Baten, 2016). Fig. 2 depicts the entire modeling and simulation framework. The more interested reader should read MOSAIC (2011) and AMSTERCHEM (2018) for more details.

The proposed model, therefore provides an equation-oriented formulation of the falling film absorber, which can be integrated with other simulation or optimization environments and take advantage of state-of-the-art solution techniques for large-scale NLPs. Furthermore, unlike the other approaches usually carried out in literature, changes on some underlying equation or on the working fluid can be made in a straightforward manner.

3. Results and discussions

This section firstly compares the modeling approach regarding the equilibrium at the interface according to the discussion in Section 2.4. Secondly, it presents the validation of the TTP

properties and of the falling film model against experimental data from literature. The validated model is then simulated and an analysis of the main mass and heat transfer resistances and the effect of inlet conditions on the process performance is performed.

3.1. Evaluation of the phase equilibrium models

The empirical and rigorous approaches to describe the equilibrium at the interface are validated against the experimental data from Clifford and Hunter (1932), who reported VLE data for the system NH_3/H_2O at temperatures up to 423.15 K and at pressures up to 20 bar. This range includes the operating conditions, $P = 6$ bar and $298 < T < 318$ K, which are used to validate our modeling approach. Fig. 3 compares the rigorous equilibrium as suggested by Prausnltz et al. (1978) and the simplified empirical correlations by Pretek and Klomfar (1995) with the experimental data from Clifford and Hunter (1932) at 6 atm and 10 atm. Both approaches can precisely describe the VLE of the mixture with deviations of the same order of magnitude for temperatures between 303.15 K and 323.15 K, which correspond the falling film operating conditions. The average relative deviations for the liquid and vapor mass fraction at 6 atm are 1.53% and 0.70%, respectively, if the empirical correlations are used, and 3.15% for the liquid phase and 0.46%, respectively, if the rigorous model is employed. The deviations at 10 atm are very similar. The empirical correlations present a slightly better fit than the rigorous VLE formulation at higher temperatures, especially for the liquid phase. This overfit might be expected since the parameters of the empirical correlations are adjusted with the same experimental data from Clifford and Hunter (1932). On the one hand, these empirical correlations usually employed in literature to model the falling film absorber are only valid for the mixture NH_3/H_2O in a pressure range from 0.02 to 20 bar. On the other hand, the rigorous model formulation is based on the thermodynamic formalism which gives flexibility to the falling film model since the VLE equations might be suited to other component mixtures in a straightforward manner. Therefore, the remaining simulations are carried out using the rigorous VLE formulation from Prausnltz et al. (1978).

3.2. Validation of the thermodynamics and transport phenomena properties

Although the mixture NH_3/H_2O is well-known to many industrial applications, the correlations to calculate their TTPs are nor clearly stated neither validated by those who model the falling film absorber (Goel and Goswami, 2005a,b; Sieres and Fernandez-Seara, 2007; Triché et al., 2016, 2017; Aminyavari et al., 2017). Aware that the deviations of the TTPs correlations might propagate to the falling film output variables, we firstly validate the TTPs against experimental data from literature in order to ensure precision of the falling film model. Viscosity, density, and thermal conductivity for the pure components and for the mixture are calculated in the temperature range from 273.15 to 373.5 K and pressure 1 to 33 bar. Table 4 summarizes the average relative deviations between experimental and simulated data. As the ammonia mass fraction at the vapor phase is above 0.99, the deviations of the mixture properties at the vapor phase are similar to the pure component deviations, therefore they are not show in Table 4 for the sake of simplicity. The small deviations indicate that the model has a very good agreement with the experimental data from literature. The correlations for specific heat capacities are validated against experimental data from literature, which cover the temperature range from 290 to 390 K for the pure component (Perry and Green, 1999; NIST, 1998) and from 280 to 360 K for the liquid mixture (Fujita et al., 2008). Table 4 summarizes the average relative deviations, indicating that the model can satisfactorily predict the specific heat. As mentioned above, the deviations for the mixture at the vapor phase are not shown since it is almost pure ammonia.

The enthalpy of the mixture is validated against experimental data from Macriss et al. (1964), which are taken between 345 K and 514 K. The average deviations are 3.49% for the liquid phase when $0.02 \leq x_{NH_3} \leq 0.99$ and 3.99% at the vapor phase when $0.93 \leq y_{NH_3} \leq 0.99$, indicating the quality of fit of the correlation used. As the partial mass enthalpies at the liquid phase for each component are obtained from the mixture's enthalpy (Eq. (7)), which is already validated, there is no need to further compare the partial mass enthalpies with experimental data. The specific enthalpies for the pure component at the vapor phase are derived from the specific heat, which is satisfactorily validated as Table 4 shows.

3.3. Model validation: falling film absorber

The model proposed here is validated against experimental data from Triché et al. (2016) at four operating conditions, which present only slight changes. The outlet variables used for validation are: liquid temperature T_L (K), coolant temperature T_C (K), ammonia mass fraction x_{NH_3} and heat absorbed by the coolant Q_C (kW). In order to ensure convergence, the minimum number of discretization points is $nd = 5$, which was compared with $nd = 10$ to check the model precision. Table 5 compares the model prediction with the experimental data for cases in which the model is discretized with $nd = 5$ and $nd = 10$. The model is able to predict the experimental data with very small deviations, capturing even the slight changes in the operating conditions. When $nd = 10$, the model is described by $(10 + 3 \cdot NC) \cdot nd = 160$ non-linear algebraic equations and the execution time is 81s in a computer with Intel (R), Core (TM) i3-3217U, RAM memory 4.00GB, operational system 64 bits. When the number of discretization points is reduced to $nd = 5$, there are $(10 + 3 \cdot NC) \cdot nd = 80$ non-linear algebraic equations and the execution time decreases to 11s. A finer discretization does not necessarily means higher precision, as might be observed in Table 5, because it results in a larger-size non-linear algebraic system, which is more difficult to converge and requires a better initialization of more iteration variables. A grid with 5 discretization points is then considered for the simulations since it ensures convergence with a great accuracy. Both approaches to compute the equilibrium at the interface, rigorous and empirical, are further compared, corroborating the good fit of the rigorous equilibrium, which gives flexibility and robustness to the model. Unlike Sieres and Fernandez-Seara (2007), who report numerical problems due to the asymptotic discontinuity in the flux's calculation (Table 5), the non-linear algebraic system is solved here successfully, further suggesting the robustness of the proposed approach.

3.4. Analysis of the mass and heat transfer phenomena

This section investigates the behavior of the falling film absorber after it has been successfully validated. Firstly,

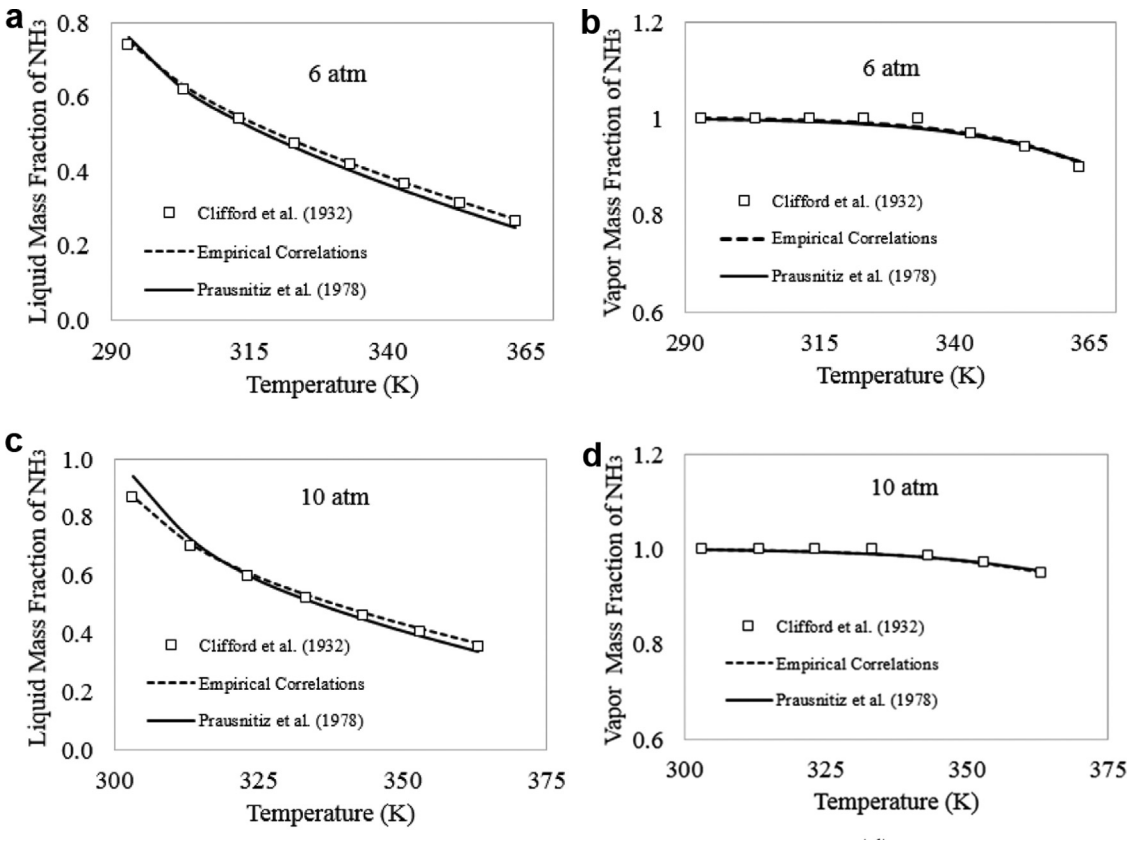

Fig. 3 – Validation of the VLE equilibrium model: (a) liquid and (b) vapor phases at 6 atm and (c) liquid and (d) vapor phases at 10 atm.

Table 4 – Average relative deviation of transport and thermodynamic properties.

Property	NH_3		H_2O		NH_3/H_2O
	Liquid	Vapor	Liquid	Vapor	Liquid
Density ($kg\,m^{-3}$) $294.5\,K < T < 343.0\,K$ $4.29\,bar < P < 33.14\,bar$	0.70%[1]	1.87%[2]	0.08%[3]	0.68%[2]	0.74%[11] @ $x_{NH_3} = 0.176$
Viscosity ($Pa\,s$) $290.0\,K < T < 340.0\,K$ $1\,bar < P < 10\,bar$	2.55%[4]	1.41%[5]	3.06%[6]	1.37%[7]	5.51%[7] @ $x_{NH_3} = 0.150$
Thermal conductivity ($W\,m^{-1}\,K^{-1}$) $273.15\,K < T < 373.5\,K$ $1\,bar < P < 10\,bar$	5.74%[8]	3.38%[9]	1.74%[10]	0.68%[7]	2.43%[9] @ $0 \leq x_{NH_3} \leq 0.27$
Specific heat capacity ($kJ\,kg^{-1}\,K^{-1}$) $290.0\,K < T < 390.0\,K$ $1\,bar < P < 15.35\,bar$	1.32%[2]	0.11%[12]	2.41%[12]	0.08%[2]	1.70%[13] @ $0.15 \leq x_{NH_3} \leq 0.84$

[1]Cragoe and Harper (1921), [2]Perry and Green (1999), [3]Aznar et al. (1984), [4]Laesecke et al. (1999), [5]Trautz and Heberling (1931), [6]Agaev et al. (1968), [7]Timrot and Par vysokih (1950), [8]Varlashkin and Thompson (1963), [9]Golubev et al. (1964), [10]Lees et al. (1898), [11]Liu et al. (2012), [12]NIST (1998), [13]Fujita et al. (2008).

the falling film absorber behavior is evaluated for the nominal case with the following inlet conditions, taken from the experimental condition reported by Triché et al. (2016): $m_V = 5.25 \cdot 10^{-3}\,kg/s$, $m_L = 1.67 \cdot 10^{-2}\,kg/s$, $T_V = 296.9\,K$, $T_L = 312.0\,K$, $x_{NH_3} = 0.46$, $y_{NH_3} = 0.995$, $P = 6.03\,bar$, $T_c = 300.20\,K$ and $m_c = 0.626\,kg\,s^{-1}$. Then, the dominant mass and heat transfer resistances are investigated in order to understand which phase (liquid or vapor) controls the mass and heat transfer phenomenon on the absorption process.

Fig. 4 illustrates temperature profiles for the liquid and vapor phases as well as the coolant and the interface along the absorber length for the nominal case. The ammonia absorption by ammonia-water solution is an exothermic process, then heat is rejected from the liquid phase to the coolant, which maintains the absorption temperatures, keeps the liquid solution far from boiling and helps to shift the equilibrium favorably in the direction of the absorption. As a result, the temperature of the liquid phase decreases from top to bottom while the coolant temperature increases from bottom to top, since it flows counter-currently. The temperature at the interface and at the liquid bulk are nearly the same indicating that the liquid-side transfer resistance is negligible. Here,

Table 5 – Validation of the falling film model against experimental data from Triché et al. (2016).

Test	nd	T_L (K)			T_C (K)			x_{NH_3}		
		Exp	Deviation (%)		Exp	Deviation (%)		Exp	Deviation (%)	
			Empirical	Rigorous		Empirical	Rigorous		Empirical	Rigorous
1	5	303.7	0.04	0.08	305.8	0.52	0.51	0.591	0.72	2.30
	10		0.28	0.37		0.31	0.01		0.68	0.63
2	5	303.5	0.31	0.57	305.5	0.21	0.04	0.588	1.48	3.47
	10		1.21	1.08		1.25	1.12		0.20	0.34
3	5	304.0	0.23	0.06	305.8	0.18	0.03	0.588	2.58	3.16
	10		1.06	0.89		1.17	1.27		0.87	1.12
4	5	303.2	0.96	0.23	305.1	0.58	0.18	0.591	0.72	3.22
	10		0.87	0.85		0.86	1.24		1.84	1.18

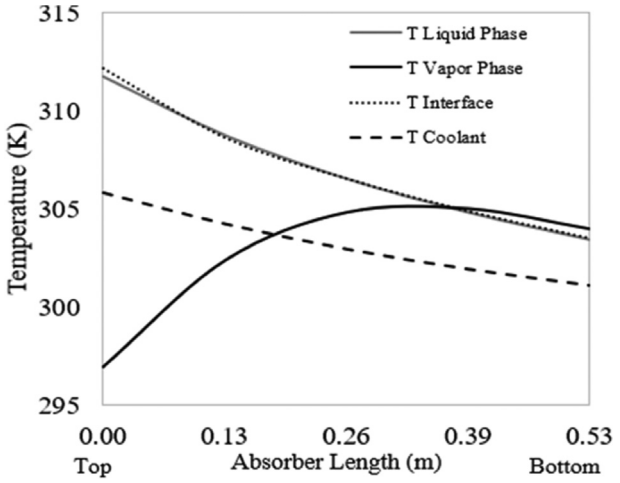

Fig. 4 – Temperature profile along the absorber length.

unlike observed by Triché et al. (2016) and Goel and Goswami (2005a), the interface temperature is not always slightly higher than the liquid temperature, what occurs due to the heat generated by the absorption at the interface. This is explained by the different approach used to compute the equilibrium at the interface because, if the empirical correlations are used to calculate the compositions at the interface, the same results from Triché et al. (2016) are observed. Here, a rigorous thermodynamic model is employed instead of empirical correlations. As discussed in Section 3.1, there is a slight difference between the empirical and rigorous correlations describing the VLE at the interface. Regarding the vapor temperature, it increases at the first section of the absorber until it reaches the interface temperature near z = 0.39 m due to the heat generated by the absorption process. After that point, since the temperature at the vapor phase is slightly higher than the interface temperature, according to the energy balance at the interface (Table 2), the heat flux is reversed and then the vapor phase slowly cools down.

Fig. 5a and b depicts the concentration profiles along the absorber. As expected, ammonia is continuously absorbed into the liquid phase as its mass fraction increases along the absorber length due to the higher ammonia content in the vapor phase. In the vapor phase, the ammonia mass fraction firstly decreases not only due to the ammonia absorption into the liquid phase but also due to the water desorption from the liquid phase into the vapor phase (Z > 1). When Z < 1, though, water is absorbed into the liquid phase so that the ammonia mass fraction in vapor phase stops changing. The same behavior has been observed by Fernandez-seara et al. (2005), Herbine and Perez-blanco (1995), and Triché et al. (2016, 2017). Fig. 5 further indicates that $y \geq y_{int}$, $x_{int} \geq x$ and $y_{int} > x_{int}$ ensuring that ammonia is continuously absorbed, as also observed by Sieres et al. (2007). The interface mass fractions (x_{int} and y_{int}) increase along the absorber as the interface temperature decreases, as shown in Figs. 4, 5a and b. This behavior might be understood with the help of the liquid-vapor phase diagram illustrated in Fig. 5c. At a given temperature at the interface, the equilibrium composition is indicated. For a lower interface temperature, the phase diagram indicates that the mass fraction of both liquid and vapor phases will increase.

The dominant resistance in heat and mass transfer is not a consensus in literature; therefore, this phenomenon is investigated here. The simplified driving force for mass transfer is the difference between the concentration at the gas phase and at the interface, $y_{NH_3} - y_{int,NH_3}$, and between the concentration at the interface and at the liquid phase, $x_{int,NH_3} - x_{NH_3}$, which are illustrated in Fig. 6 for the nominal case. Since the gradient at the liquid phase is much higher than at the vapor phase, the overall mass transfer resistance is mostly due to the liquid phase. Analyzing the mass transfer parameters for the vapor, $F_V = K_V \cdot \rho_V$, and liquid phase, $F_L = K_L \cdot \rho_L$ in Fig. 6b, we arrive to the same conclusion: the liquid side controls the mass transfer since $F_L > F_V$ along the falling film. These findings corroborate the conclusion from Kim et al. (2003), Perez-Blanco (1988) and Goel and Goswami (2005a,b). Triché et al. (2017) and Goel and Goswami (2005a) affirm that the heat transfer resistance at the vapor phase ($1/\alpha_V$) is large whereas at the liquid phase ($1/\alpha_L$) is negligible. Fig. 6c shows the heat transfer coefficients in liquid and vapor phases, indicating that the resistance at the vapor phase is two orders of magnitude greater than the resistance at the liquid solution.

3.5. *Analysis of the inlet conditions in the absorption performance*

The falling film absorber has the goal to absorb the refrigerant (ammonia) from the vapor phase, concentrating the solution. This section, then, investigates the effect of some inlet variables on the ammonia mass fraction at the liquid phase, x_{NH_3}. This investigation might be useful to better understand the variables that greater influence the ammonia content at the outlet stream. Based on the conclusion that the dominant mass transfer resistance occurs at the liquid side, the following inlet variables are investigated: liquid and coolant inlet temperature, $T_{L,in}$ and $T_{c,in}$, inlet mass fraction of ammonia at the liquid phase $x_{NH_3,in}$ and coolant inlet mass flowrate $m_{c,in}$. Fig. 7a shows the ammonia mass fraction at liquid phase along

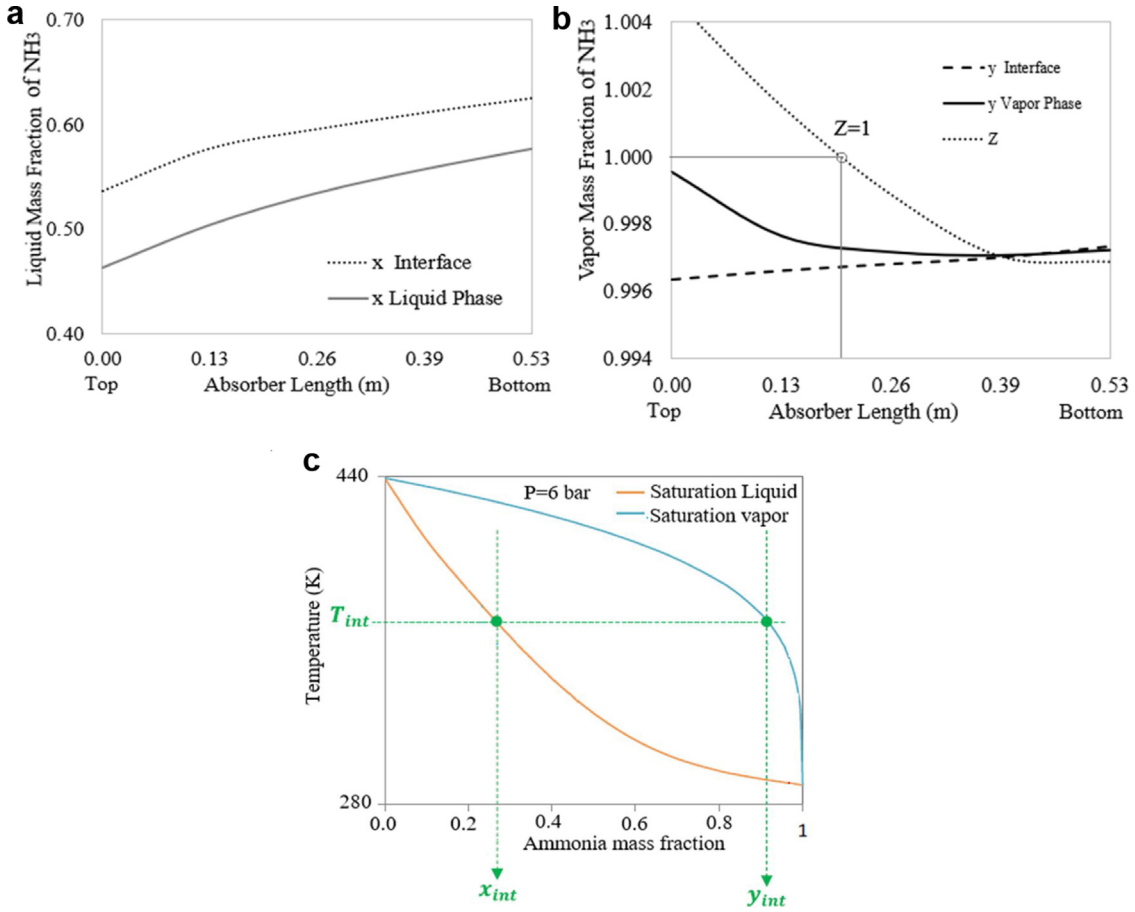

Fig. 5 – Liquid (a) and vapor (b) phase concentration profiles along the absorber length, (c) liquid-vapor phase diagram for NH_3/H_2O at 6 bar.

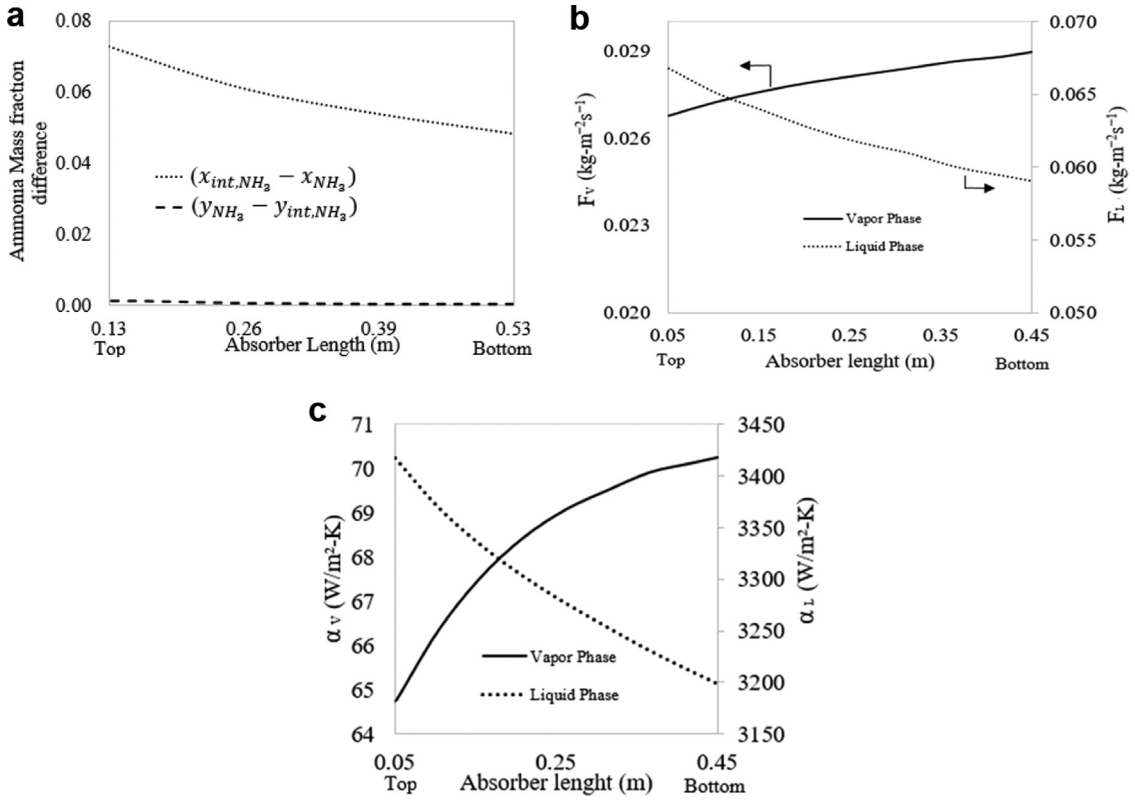

Fig. 6 – (a) Ammonia mass fraction gradients and (b) correlations with mass transfer coefficients (F_V and F_L) and (c) heat transfer coefficients for the vapor and liquid phases and.

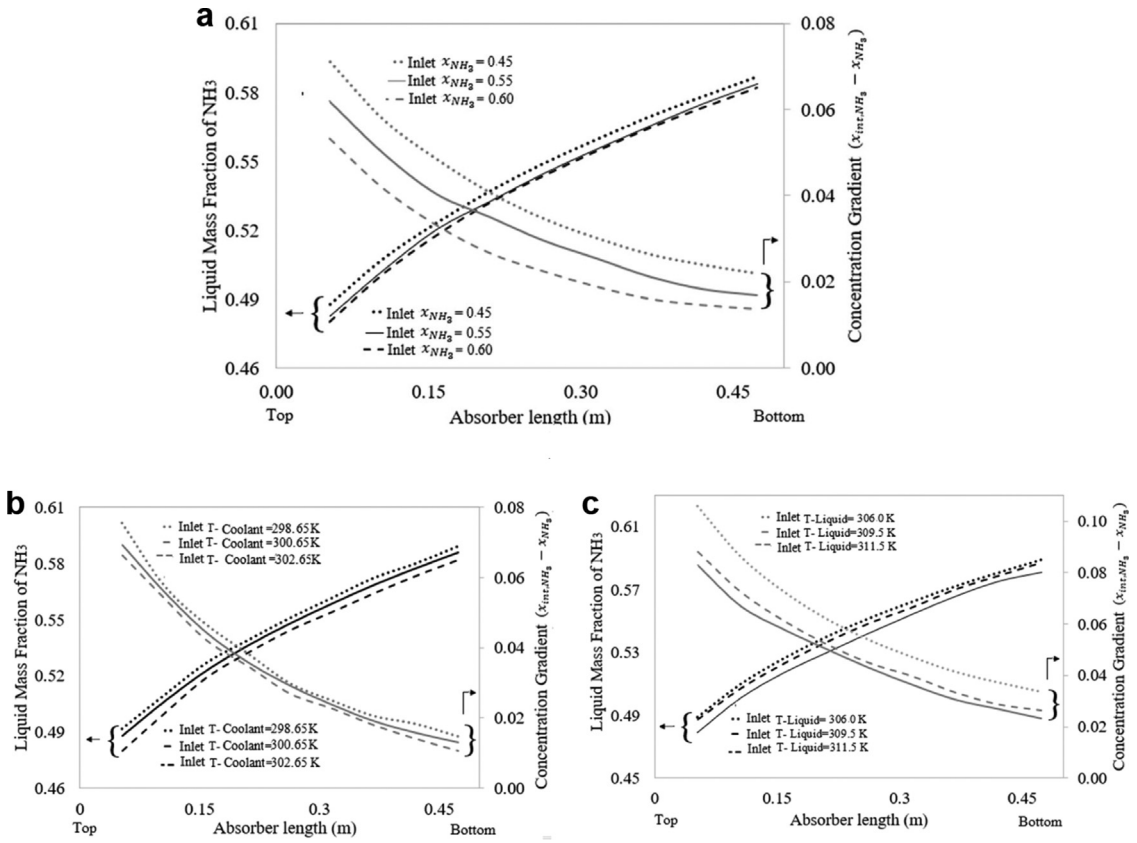

Fig. 7 – (a) Analysis of the liquid inlet mass fraction of ammonia along the absorber, Influence of coolant (b) and liquid (c) inlet temperature on absorption of ammonia.

the absorber length for different $x_{NH_3,in}$ as well as the ammonia mass fraction gradient between the liquid interface and the liquid phase. The lower the inlet mass fraction of ammonia, the higher is the gradient, since the concentration at the vapor phase has not changed. This favors the ammonia absorption into the liquid phase, yielding an increase in the ammonia mass fraction at the liquid phase.

The influence of coolant and liquid inlet temperatures on the absorption of ammonia are illustrated in Fig. 7b and c, respectively. The concentration gradients are greater at the top because of the more pronounced difference in ammonia concentration between the liquid and vapor phases. At the top occurs the lowest concentrations of ammonia in the liquid phase, while the vapor stream feeds the top with $y_{NH_3} = 0.995$. As the absorption occurs along the falling film, the liquid phase gets richer in ammonia so that the concentration gradient decreases. The coolant inlet temperature ranges from 298.5 to 300.5 K, according to Goel and Goswami (2005a), as it covers typical thermal conditions of the cooling units for this process. The lower the inlet coolant temperature, the lower will be the liquid temperature along the absorber's length since the heat generated by the absorption is transferred to the coolant. As a result, the higher will be the ammonia content at the interface, according the phase diagram in Fig. 5c, resulting in a higher concentration gradient between the interface and the bulk phases, as illustrated by Fig. 7a and b. The same behavior is observed for decreasing liquid inlet temperatures. Analyzing the coolant inlet mass flow rate, it has the same effect as the decrease in the inlet coolant temperature since a higher flow rate increases the heat flux from the liquid to the coolant. For the sake of simplicity, the profiles are not shown here. The sensitive analyses indicate that lower inlet coolant temperature or lower liquid inlet temperature allows a higher ammonia absorption, as desired. These results, therefore, might be useful to control or to maximize the ammonia content at the outlet stream.

4. Conclusion

This paper presents a model of a plate falling film absorber, which is solved using an equation-oriented approach. The model consists of mass and energy balances, equilibrium heat and mass transfer equations as well as thermodynamic and transport property calculations. The finite differences method is applied and the resulting set of algebraic non-linear equations is solved simultaneously by a residual minimization method. The model has been successfully validated with data from literature, showing a maximum relative deviation of 3.47% For the considered operational conditions, results indicate that the overall resistance for mass transfer along the falling film absorber is controlled by the liquid phase whereas the coolant side heat transfer resistance dominates the overall heat transfer resistance.

Additionally, this paper proposes computing the phase equilibrium for the binary NH_3-H_2O system using the thermodynamic formalism. This approach is compared with the usual practice in literature, which uses empirical correlations. The results show that both approaches are able to describe the compositions at the interface under a broad range of operating conditions. The empirical correlations, though, are restricted for the operating conditions where the parameters were validated and for the ammonia and water mixture. The rigorous vapor–liquid equilibrium at the interface, on the other hand, gives flexibility to the model since the thermodynamic model might be changed in a straightforward manner to better rep-

resent the mixture and the operating conditions accordingly. The computation of the TTP using CAPE-open interfaces is another relevant feature of the proposed approach since it gives further flexibility to the model since the correlations that describe the TTP might be easily changed to better fit the system investigated. Additionally, we not only detail the modeling of the TTP but also validate their correlations prior to incorporating them into the falling film model.

The results corroborate that the proposed modeling approach can efficiently solve the falling film model on the basis of a unique set of differential algebraic equations. The equation-oriented approach does not need a tailored sequential algorithm neither fails with the numerical problems reported in literature. Therefore, the simultaneous approach proposed here is more robust and more flexible since it can be extended to other mixtures and integrated to a process flowsheet or optimization problems. This study motivates future applications of this numerical approach in absorbers with different geometries, as vertical and horizontal pipes, packed columns, and with other working fluids as well. Furthermore, the implementation of this model in an equation-oriented fashion enables its further utilization for simultaneous large-scale flowsheet optimizations, allowing the optimal design and operation of absorption refrigeration machines.

Conflicts of interest

The authors declare no conflicts of interest.

Acknowledgments

The authors acknowledge CAPES (Coordenação de Aperfeiçoamento de Pessoal de Nível Superior) and CNPq (Conselho Nacional de Desenvolvimento Científico e Tecnológico) for the financial support.

Appendix A

The following correlations are used to calculate some Thermodynamics and Transport Phenomena Properties of NH_3, H_2O and NH_3/H_2O mixture, such as: specific heat and binary diffusivity coefficient.

- Specific heat of ammonia and water in vapor phase, $Cp_{V,i}$ ($J\,mol^{-1}\,K^{-1}$) are calculated by (Van Ness et al., 2007):

$$\frac{Cp_{V,i}}{R} = A + BT + CT^2 + DT^{-2} \tag{A.1}$$

where A, B, C, D are parameters (Van Ness et al., 2007), T (K) is temperature and R ($J\,mol^{-1}\,K^{-1}$) is the gas constant.

- Specific heat of ammonia and water in liquid phase ($J\,mol^{-1}\,K^{-1}$), are respectively computed by (Perry, 1999):

$$Cp_{L,NH_3} = \frac{{C_1}^2}{t} + C_2 - 2C_1C_3t - C_1C_4t^2 - \frac{C_3^2t^3}{3} - \frac{C_3C_4t^4}{2} - \frac{C_4^2t^5}{5} \tag{A.2}$$

$$Cp_{L,H_2O} = C_1 + C_2T + C_3T^2 + C_4T^3 + C_5T^4 \tag{A.3}$$

where T (K) is temperature, C_1, C_2, C_3, C_4 and C_5 are parameters (Perry, 1999), $t = 1 - T_r$. T_r, $T_r = T/T_c$ and T_c is critical temperature (K).

- Specific heat of the liquid and vapor mixtures are calculated according to (Conde, 2006; Prata, 2012; Triché, 2016):

$$C_{PL} = x_{NH_3}C_{PL,NH_3} + x_{H_2O}C_{PL,H_2O} \tag{A.4}$$

$$C_{PV} = y_{NH_3}C_{PV,NH_3} + y_{H_2O}C_{PV,H_2O} \tag{A.5}$$

where x and y are mass fractions at the liquid and vapor phase, respectively.

- The binary diffusivity coefficient for the liquid mixture can be calculated by (Conde, 2006):

$$D_L = 117.282 \cdot 10^{-18} T \frac{\sqrt{\Psi_m M_m}}{\mu_m V_{diff}^{0.6}} \tag{A.6}$$

where T (K) is temperature, μ_m (Pa s) is the dynamic viscosity, M_m ($g\,mol^{-1}$) is the mixture molecular weight, V_{diff} ($cm^3\,mol^{-1}$) is the molar volume from Conde (2006) and is the mixture association factor from Wilk and Chang, 1955.

- The binary diffusivity coefficient for the vapor phase can be computed by the Chapman-Enskog equation (Bird et al., 2006):

$$D_V = 0.0018583\sqrt{T^3\left(\frac{1}{M_{NH_3}} + \frac{1}{M_{H_2O}}\right)}\left(\frac{1}{P\sigma_{NH_3,H_2O}\Omega_D}10^{-4}\right) \tag{A.7}$$

where T (K) is temperature, M_{NH_3} and M_{H_2O} are the molecular weights for ammonia and water, respectively, P (atm) is pressure, Ω_D is a collision integral and σ_{NH_3,H_2O} (Å) is the molecular diameter, both of them from Hirschfelder et al. (1954).

References

Agaev, N.A., Usibova, A.D., Dokl, A., Nauk, A.Z., 1968. Viscosity of ordinary and heavy water at high pressures in the temperature range from 0 to 150 °C. Soviet Phys. Doklady 13, 334–337.

Aminyavari, M., Aprile, M., Toppi, T., Garone, S., Motta, M., 2017. A detailed study on simultaneous heat and mass transfer in an in-tube vertical falling film absorber. Int. J. Refrig. 80, 37–51.

AMSTERCHEM CAPE-OPEN Thermo Import, https://www.amsterchem.com/matlabthermo.html (accessed 26.03.18).

Aznar, M.A., Gimeno, R.J., perez, G.D., Carrasco, G., Afinidad, J.L., 1984. Density and excess volume of alkyl pyridine-water systems. Chem. Eng. Data 41, 355.

Bird, B., Stewart, W., Lightfoot, E., 2006. Transport Phenomena, Revised, second ed. JohnWiley & Sons, Inc.

Bohra, L.K., 2007. Analysis of Binary Fluid Heat and Mass Transfer in Ammonia-Water Absorption. PhD Dissertation Presented to The Academic Faculty. Georgia Institute of Technology.

Chen, J., Bo, H., Ma, S., Chen, X.Z.L., 2010. Numerical simulation on the falling film absorption process in a counter-flow absorber. Chem. Eng. J. 156, 607–612.

Chilton, T.H., Colburn, A.P., 1934. Mass transfer (absorption) coefficients prediction from data on heat transfer and fluid friction. Ind. Eng. Chem. 26, 1183–1187.

Clifford, I.L., Hunter, E., 1932. The system ammonia-water at temperatures up to 150 °C and at pressures up to twenty atmospheres. J. Phys. Chem. 37, i01–i118.
CoLan documentation. (2011, May). Retrieved from http://www.colan.org/.
Conde, M., 2006. Thermophysical Properties of Ammonia-Water Mixtures for the Industrial Design of Absorption Refrigeration Equipment. M. CONDE Engineering.
Cosenza, F., Vliet, G.C., 1990. Absorption in falling water/LiBr films on horizontal tubes. ASHRAE Trans. 96, 693–701.
Cragoe, C.S., Harper, D.R., 1921. Specific volume of liquid ammonia. Sci. Pap. Bur. Stand. (U. S.) 17, 287–315.
Deng, S.M., Ma, W.B., 1999. Experimental studies on the characteristics of an absorber using LiBr/H2O solution as working fluid. Int. J. Refrig. 22, 293–301.
Din, F., 1956. Thermodynamic Functions of Gases, vol. 1. Butterworths, London.
Edwards, T.J., Newman, J., Prausnitz, J.M., 1975. Thermodynamics of aqueous solutions containing volatile weak electrolytes. AIChE J. 21, 248–259.
Edwards, T.J., Maurer, G., Newman, J., Prausnitz, J.M., 1978. Vapor–liquid equilibria in multicomponent aqueous solutions of volatile weak electrolytes. AIChE J. 24, 966–976.
Fernandez-seara, J., Sieres, J., Rodriguez, C., Vazquez, M., 2005. Ammonia–water absorption in vertical tubular absorbers. Int. Therm. Sci. 44, 277–288.
Fujita, I., Suzuki, T., Uematsu, M.J., 2008. Chem. Thermodyn. 40, 260–264.
Goel, N., Goswami, D.Y., 2005a. Analysis of a counter-current vapor flow absorber. Int. J. Heat Mass Transf. 48, 1283–1292.
Goel, N., Goswami, D.Y., 2005b. A compact falling film absorber. J. Heat Transf. 127, 957–965.
Golubev, I.F., Sokolova, V.P., Teploenergetika, 1964. Thermal conductivity of ammonia at various temperatures and pressures. J. Heat Transf. 11, 64–67.
Gommed, K., Grossman, G., Koenig, M.S., 2001. Numerical study of absorption in a laminar falling film of ammonia-water. ASHRAE Trans. 107, 453–462.
Grossman, G., 1983. Simultaneous heat and mass transfer in film absorption under laminar flow. Int. J. Heat Mass Transf. 26, 357–371.
Ariyadi, H.M., Coronas, A., 2016. Absorption capacity of ammonia into ionic liquids for absorption refrigeration applications. J. Phys.: Conf. Ser. 745, 032105.
Habib, H.M., Wood, B.D., 2001. Simultaneous heat and mass transfer in film absorption with the presence of non-absorbable gases. J. Heat Transf. 123, 984–989.
Herbine, G.S., Perez-blanco, H., 1995. Model of an ammonia–water bubble absorber. ASHRAE ASHRAE Tech. Data Bull. 11, 102–110.
Hirschfelder, J., Curtiss, C.F., Bird, R.B., 1954. Molecular Theory of Gases and Liquids. Wiley, New York, ISBN0471400653.
Ho, J.C., Islam, M.R., Wijeysundera, N.E., 2004. Simplified models for coupled heat and mass transfer in falling-film absorbers. Int. J. Heat Mass Transf. 47, 395–406.
Killion, J.D., Garimella, S., 2001. A critical review of models of coupled heat and mass transfer in falling-film absorption. Int. J. Refrig. 24 (8), 755–797.
Krichevsky, I.R., Kasarnovsky, J.S., 1935. Thermodynamical Calculations of Solubilities of Nitrogen and Hydrogen in Water at High Pressures. J. Am. Chem. Soc. 57, 2168–2171.
Kakaç, S., Aung, W., Shah, R.K., 1987. Handbook of Single-phase Convective Heat Transfer. Wiley, NewYork.
Kang, Y.T., Akisawa, A., Kashiwagi, T., 2000. Analytical investigation of two different absorption modes: falling film and bubble types. Int. J. Refrig. 23, 430–443.
Kang, Y.T., Kashiwagi, T., Christensen, R.N., 1998. Ammonia-water bubble absorber with a plate heat exchanger. ASHRAE Trans. Pt. 1B, 1565–1575.
Kim, B., 1998. Heat and mass transfer in a falling film absorber of ammonia-water absorption systems. Heat Transf. Eng. 19 (3), 53–63.
Kim, H.Y., Saha, B.B., Koyama, S., 2003. Development of a slug flow absorber working with ammonia–water mixture: part II–data reduction model for local heat and mass transfer characterization. Int. J. Refrig. 26, 698–706.
Laesecke, A., Lueddecke, T.O.D., Hafer, R.F., Morris, D.J., 1999. Viscosity measurements to ammonia, R32, and R134a. Vapor buoyancy and radial acceleration in capillary viscometers. Int. J. Thermophys. 20, 401–434.
Lázaro-Colán, V.A., 2012. Experimental Study of an Absorption Column of Water Vapor and Ammonia in Water, PhD Thesis. Federal University (USP), Sao Paulo, Sao Paulo, Brazil.
Lees, C.H., Philos, Trans, R., 1898. On the thermal conductivities of single and mixed solids and liquids and their variation with temperature. Soc. Lond. Ser. A 191, 339–440.
Leite, B., 2015. Modeling of the Absorber and the Generator of Ammonia/Water Heat Absorption Refrigeration Cycle Base on the Falling Film Technology on Inclined Plates. Master Thesis. Sao Paulo, Federal University (USP), Sao Paulo, Brazil.
Lin, P., Xia, W.R.Z., 2011. Numerical investigation of a two-stage air-cooled absorption refrigeration system for solar cooling: cycle analysis and absorption cooling performances. Renew. Energy 36, 1401–1412.
Liu, J., Wang, S., Hartono, A., Svendsen, H.F., 2012. Solubility of N2O in and density and viscosity of aqueous solutions of piperazine, ammonia, and their mixtures from 283.15 to 323.15 K. Chen. C.J. Chem. Eng. Data 57 (9), 2387–2393.
Macriss, R.A., Eakin, B.E., Ellington, R.T., Huebler, J., 1964. Physical and thermodynamic properties of ammonia-water mixtures. IGT Res. Bull. 34.
Merchan, V.A., Esche, E., Fillinger, S., Tolksdorf, G., Wozny, G., 2015. Computer-aided process and plant development–a review of common software tools and methods and comparison against an integrated collaborative approach. Chem. Ingeniuer Tech. 88, 50–69.
Miller, W.A., Keyhani, M., 2001. The correlation of simultaneous heat and mass transfer experimental data for aqueous lithium bromide vertical falling film absorption. J. Sol. Energy Eng. 123, 30–42.
Mittermaier, M., Ziegler, F., 2015. Theoretical evaluation of absorption and desorption processes under typical conditions for chillers and heat transformers. Int. J. Refrig. 59, 91–101.
MOSAIC documentation (October, 2011). Retrieved from http://www.mosaic-modeling.de.
Perez-Blanco, H.A., 1988. A model of an ammonia-water falling film absorber. ASHRAE Trans. 94 (1), 467–483.
Perry, R.H., Green, D.W. (Eds.), 1999. Perry's Chemical Engineers' Handbook. McGraw-Hill, New York.
Potnis, S.V., Anand, G., Gomezplata, A., Erickson, D.C., Papar, R.A., 1997. GAX component simulation and validation. ASHRAE Trans. 1, 454–459.
Prata, J.E., 2012. Modeling of a Falling Film Absorber for a Refrigeration Cycle by Absorption of Ammonia and Water. Master Thesis. Sao Paulo, Federal University (USP), Sao Paulo, Brazil.
Prausnltz, J.M., Edwards, T.J., Newman, J., 1978. Thermodynamics of vapor–liquid equilibria for the ammonia-water system. Ind. Eng. Chem. Fundam. 17, 264–269.
Pretek, J., Klomfar, J., 1995. Simple functions for fast calculations of selected thermodynamic properties of the ammonia-water system. Int. J. Refrig. 18 (228), 234.
Rosa, L.S., Pontes, K.V., Penteado, A.T., Tolksdorf, G., Esche, E., Repke, J.-U., 2018. Using MOSAICmodeling and CAPE-OPEN interfaces for property calculations in MATLAB. Blucher 1, 4392–4395.
Seader, D., Henley, E.J., 1998. Separation Process Principles Published. Wiley, New York.
Sieres, J., Fernandez-seara, J., 2007. Modeling of simultaneous heat and mass transfer processes in ammonia–water absorption systems from general correlations. Heat Mass Transfer 44, 113–123.
Sieres, J., Fernández-seara, J., Uhía, F., 2007. Analysis of an air cooled ammonia–water vertical tubular absorber. Int. J. Therm. Sci. 46, 93–103.

Timrot, D.L., Par vysokih, 1950. Steam of high parameters in energetics: Properties of water steam. Parametr. Energ. 72, 767–778.
Tolksdorf, G., Esche, E., Wozny, G., Repke, J.-U., 2019. Customized code generation based on user specifications for simulation and optimisation. Comput. Chem. Eng. 121, 670–684.
Trautz, M., Heberling, R., 1931. Viscosity of ammonia & its mixture with hydrogen, nitrogen, ethylene, ANN. Physik 10, 155–177.
Treybal, R.E., 1980. Mass Transfer Operations. McGraw-Hill, New York.
Triché, D., Bonnota, S., Perier-muzeta, M., Boudéhenna, F., Demaslesa, H., Caney, N., 2016. Modeling and experimental study of an ammonia-water falling film Absorber SHC 2015. Int. Conf. Sol. Heat. Cool. Build. Ind. Energy Proc. 91, 857–867.
Triché, D., Bonnota, S., Perier-muzeta, M., Boudéhenna, F., Demaslesa, H., Caney, N., Perier-muzet, M., 2017. Experimental and numerical study of a falling film absorber in an ammonia-water absorption chiller. Int. J. Heat Mass Transf. 111, 374–385.
Triché, D., 2016. Numerical and Experimental Study of Coupled Mass and Heat Transfers in the Absorber of an Ammonia-Water Absorption Machine. PhD Thesis. Université Grenoble Alpes, France.
Van Baten, J., 2016. COCO Cape Open to Cape Open Simulation Environment, www.cocosimulator.org.
Van Ness, H.C., smith, J.M., Abbott, M.M., 2007. Introduction to Chemical Engineering Thermodynamics, 7th Edition. McGraw Hill Professional, New York.
Varlashkin, P.G., Thompson, J.C.J., 1963. Thermal conductivity of liquid ammonia. Chem. Eng. Data 8, 526.
Flori, M., Vîlceanu, L., 2012. Performance characteristics of vapor compression refrigeration systems. Ann. Faculty Eng. Hunedoara-Int. J. Eng. 2, 145–148.
Vyazovov, V.V., 1940. A theory of absorption of slightly soluble gases by liquid films. I. Tech. Phys. 10, 1519–1532.
Wilke, C.R., Chang, P., 1955. Correlation of diffusion coefficients in dilute solutions. AIChE J. 1 (2), 264–270.
Wilke, W., 1962. Wärmeübergang an Rieselfilme. VDI-Fors-Chungsheft 490, B28.
Yih, S.M., 1986. Modeling heat and mass transport in falling film liquid films. In: P: Cheremisinoff, N. (Ed.), Handbook of Heat and Mass Transfer: Mass Transfer and Reactor Design. Gulf Publishing Company 5, pp. 111–120.
Ziegler, B., Trepp, C., 1984. Equation of state of ammonia–water mixtures. Int. J. Refrig. 7, 101–106.